

Lawrence Berkeley National Laboratory

Chemical Sciences

Title

Cobalt carbonate hydroxide superstructures for oxygen evolution reactions

Permalink

<https://escholarship.org/uc/item/5d91c5qb>

Journal

Chemical Communications, 53(57)

ISSN

1359-7345

Authors

Zhang, Simin
Ni, Bing
Li, Haoyi
[et al.](#)

Publication Date

2017-07-13


DOI

10.1039/c7cc04604a

Peer reviewed



Cobalt carbonate hydroxide superstructures for oxygen evolution reactions†

Simin Zhang, Bing Ni, Haoyi Li, Haifeng Lin, Huihui Zhu, Haiqing Wang and Xun Wang *

Cite this: *Chem. Commun.*, 2017, 53, 8010

Received 14th June 2017,
Accepted 20th June 2017

DOI: 10.1039/c7cc04604a

rsc.li/chemcomm

A novel three-dimensional (3D) superstructure of cobalt hydroxide carbonate assembled from nanoneedles has been synthesized via a facile hydrothermal method. Furthermore, we tested the electrocatalytic oxygen evolution reaction performance, which demonstrated that the superstructure exhibited high catalytic activity, achieving 10 mA cm⁻² at a low overpotential of merely 240 mV.

Water splitting offers an attractive chemical method for storing renewable energy in the form of hydrogen.¹ However, the oxygen evolution reaction (OER) is usually more sluggish than the hydrogen evolution reaction (HER) during water splitting, thus developing efficient OER catalysts is important for the improvement of the efficiency of the electro/photocatalytic water splitting system.² This has greatly stimulated numerous efforts to explore novel OER catalysts. It is recognized that RuO₂ and IrO₂ can exhibit excellent catalytic activity in the OER.³ However, they are rare in the earth's crust, expensive and suffer from corrosion to some extent.^{4,5} It is urgent to develop earth-abundant, inexpensive and stable catalysts for OER.

In recent years, lots of compounds of cobalt (Co₃O₄, CoO, Co(OH)₂, CoP *etc.*) have been applied as OER catalysts and found to be performing better and better.^{6–15} However, the electrocatalytic activities of cobalt-based materials are still less competitive compared to those of precious metal electrocatalysts.¹⁶ Yury *et al.* have demonstrated that the resultant self-supported electrodes are highly active toward electrocatalysis in terms of the onset potentials, exchange current densities and Tafel slopes.^{17–20} And an appropriate structure of a cobalt-based material can enhance the electrocatalytic activity for OER.²¹ In considering these findings, we try to synthesize a novel cobalt carbonate hydroxide superstructure (CCHS) and fabricate a self-supported electrode using carbon paper (CP) as the carrier. This kind of integrated 3D electrode could not only enhance the electron transport and

exposed surface area, but also achieve a greater current density which is favorable for practical applications.^{22,23} We loaded the samples synthesized under different conditions on the CP for the characterization of the electrocatalytic oxygen evolution reaction (OER). The results demonstrate that the CCHS loaded on the carbon paper (CCHS/CP) shows good activity for the OER, delivering a current density of 10 mA cm⁻² at an overpotential of ~240 mV with a Tafel slope of 82.06 mV per decade and keeping long-term stability. These results further prove that the development of a nanostructure suitable for OER is of great importance for improving the electrocatalytic performance.

In a typical synthesis of the CCHS, we used cobalt chloride hexahydrate (CoCl₂·6H₂O) as the metal source, urea (CO(NH₂)₂) as the precipitant, sodium glycolate (C₂H₃NaO₃) as the surfactant and deionized water and absolute ethanol as solvents under hydrothermal conditions at 150 °C for 12 h (details in the ESI†). The 3D superstructure is based on the assembly of 1D nanoneedles. Fig. 1a–e present the typical scanning electron microscopy (SEM) images and transmission electron microscopy (TEM) images of the 3D superstructure taken at different magnifications. The SEM images in Fig. 1a and b show that the products are pure micrometer-sized 3D superstructures typically with diameters of about 4 μm. The flower-like 3D superstructures are based on 2D layered petals, which are constructed from 1D nanoneedles. The TEM images (Fig. 1d and e) and the enlarged SEM image (Fig. 1c) reveal that the superstructure is assembled from many nanoneedles and the order of the assembly is relatively high. The nanoneedles are uniform with a width about 20 nm. In addition, the nanoneedles in the same plane are arranged in three main directions, and the angle between the adjacent two directions is near 60°. This kind of hierarchically assembled superstructure might be beneficial for effective electrolyte transport, electron transfer, ion transport, active site accessibility and long-term stability.

The crystalline structure, details of the surface and elemental distribution were investigated using high-resolution transmission electron microscopy (HRTEM), scanning transmission electron microscopy (STEM) and element mapping, respectively. As shown

Key Lab of Organic Optoelectronics and Molecular Engineering Department of Chemistry Tsinghua University, Beijing 100084, China.

E-mail: wangxun@mail.tsinghua.edu.cn

† Electronic supplementary information (ESI) available. See DOI: 10.1039/c7cc04604a

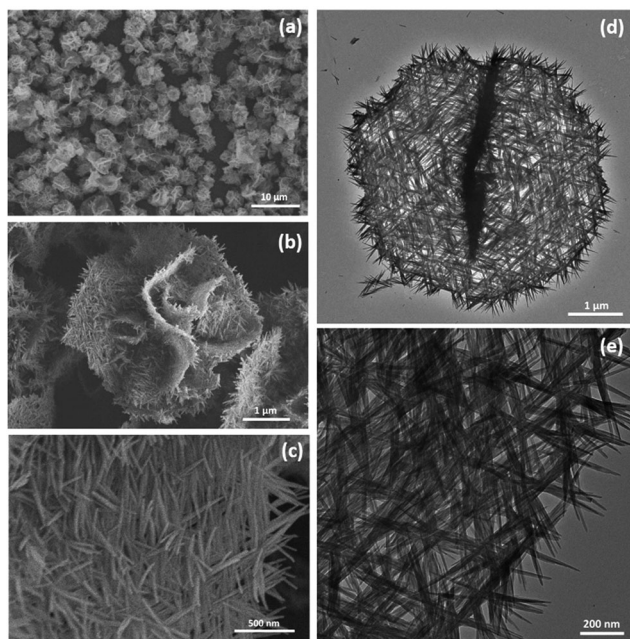


Fig. 1 (a–c) SEM images and (d) and (e) TEM images of CCHS with different magnifications.

in Fig. 2a, the nanoneedles stack up into a layered structure. Fig. 2b indicates that the nanoneedles are poorly crystalline and display several disordered crystal planes as shown in the white squares, and the corresponding fast Fourier transform (FFT) patterns are shown in the upper-left insets of Fig. 2b. The lattice fringes in squares A, B and C can be indexed to the (220), (221) and (040) crystal planes of the cobalt carbonate hydroxide (CCH) phase. And the STEM images (Fig. 2c) prove that the

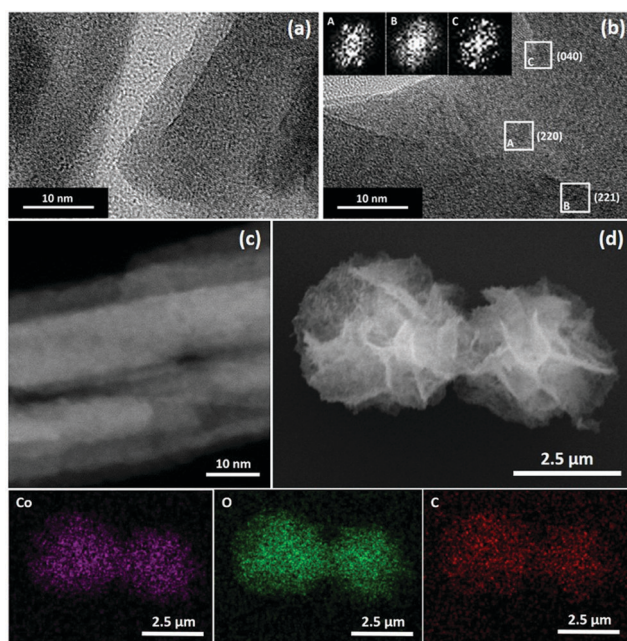


Fig. 2 (a and b) HRTEM images and the FFT patterns in the inset of (b). (c) The STEM image and (d) the element mapping of the CCHS.

surfaces of the nanoneedles are rather rough. What's more, the Co, O and C atoms are distributed uniformly in the CCHS, as shown in the element mapping (Fig. 2d).

In order to investigate the formation mechanism of the superstructure, we performed a series of time-dependent experiments. All of the synthesis conditions were the same except the reaction time. Fig. S1a–d (ESI[†]) show the TEM images of the products synthesized at 150 °C for 3 h, 6 h, 9 h and 15 h, respectively, and it is a self-assembly process obviously. First, some nanoneedles overlapped with each other and formed the frame of the structure. Then, some other nanoneedles filled the vacancy in the frame in an orderly manner to form the 3D superstructure. This is a process that grows from 1D to 2D and 3D. It is worth noting that if the reaction time is increased continuously, the superstructure becomes thicker. This observation demonstrates that nanoneedles continue to assemble together. Fig. S1e and f (ESI[†]) show the TEM images of the products synthesized at 120 °C and 180 °C for 12 h. The products synthesized at 120 °C for 12 h are disordered aggregates of nanoneedles and the products synthesized at 180 °C for 12 h are like some broken superstructures, which suggests that an excessively low temperature may lead to aggregation while an excessively high temperature may lead to destruction. The self-assembly process to form the CCHS may be driven by the interaction between sodium glycolate and the surface groups of the CCHS, and this interaction requires suitable temperature and time.

The compositions of the products were investigated through X-ray diffraction (XRD), X-ray photoelectron spectroscopy (XPS) and elemental analysis. There is no clear diffraction peak in the XRD patterns (Fig. S2, ESI[†]), but some characteristic peaks assigned to CCH appear. The unclear diffraction peaks suggest that the synthesized CCH presents weak crystallinity. In order to verify the compositions of the products, we performed elemental analysis (Table S1, ESI[†]). This shows that the elemental proportions of C and Co are nearly consistent with those of cobalt carbonate hydroxide, but the proportion of H in the product is much higher than that of cobalt carbonate hydroxide, which might be attributed to crystalline water. High-resolution XPS spectra of Co 2p, O 1s and C 1s are displayed in Fig. S3 (ESI[†]). The XPS results confirm the presence of Co²⁺, the bonds of oxygen in water, carbonate anions and hydroxyl, and the bonds of carbon in carbonate anions, C=O bonds, C–O bonds and C–C bonds.^{24–26} All these results illustrate that the as-prepared products are typical CCHs. CCH is a kind of layered material with Co(OH)⁺ as the positively charged layer, CO₃²⁻ as the counter anion and H₂O as the solvation molecule,²⁷ and it has good compatibility with electrolytes due to its good hydrophilicity.

Then the OER performance of the CCHS was evaluated, and some other comparative catalysts were also evaluated. We loaded the samples on a piece of clean CP (1 × 2 cm²) to fabricate the working electrode. The OER activities of the as-fabricated electrode are evaluated in a 1 M KOH solution saturated with O₂ (details in the ESI[†]). The CCHS/CP shows a better OER performance than bare CP and IrO₂/CP (Fig. 3a), exhibiting a low overpotential of merely ~240 mV to reach 10 mA cm⁻². In contrast, the bare CP shows a negligible current density and

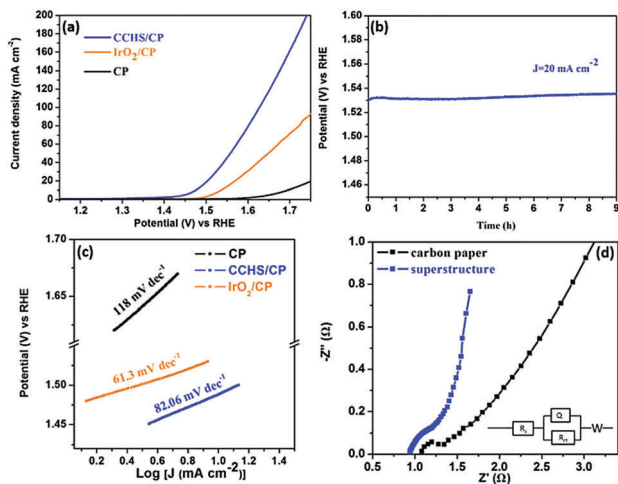


Fig. 3 (a) The polarization curves of the CCHS/CP, CP and IrO₂/CP. (b) The chronopotentiometric curve of the CCHS/CP at the current density of 20 mA cm⁻². (c) Tafel slopes of the CCHS/CP, CP and IrO₂/CP. (d) EIS spectra of the CCHS/CP and the CP.

IrO₂/CP shows a much lower current density at the same overpotential, which further confirms the high OER activity of the CCHS/CP. The chronopotentiometric curve (Fig. 3b) proves that the CCHS/CP shows not only excellent OER catalytic activity but also good stabilization, which may benefit from the mechanical stability of the integrated CCHS/CP electrode. The Tafel slopes (Fig. 3c) were tested to investigate the mechanism of OER catalysis subsequently, which are often influenced by the electron and mass transport. The CCHS/CP shows a lower Tafel slope of 82.06 mV dec⁻¹ compared to that of CP, which might be attributed to the fastest electron transport on the superstructure.

Fig. 3a and 4a show that there is little difference in the overpotentials as the CCHS/CP and different samples measured achieve 10 mA cm⁻², but there is obvious difference in the growth rate of the current density. The CCHS/CP exhibits the

highest OER catalytic activity. To reach a current density of 150 mA cm⁻², the CCHS/CP requires an overpotential of 450 mV, which is 70, 50, 40, and 30 mV less than those of the samples synthesized at 180 °C for 12 h, 150 °C for 6 h, 150 °C for 15 h and 120 °C for 12 h, respectively. In addition, the OER catalytic activities of all the samples are much better than the activities of the bare CP and IrO₂/CP. Moreover, as shown in the electrochemical impedance spectroscopy (EIS) spectra, the CCHS/CP exhibits the lowest charge-transfer resistance compared to those of the other samples (Fig. 3d, ESI[†]), indicating its superior charge transport kinetics.^{28,29} The electrochemically active surface area (ECSA) for each product was estimated from the electrochemical double-layer capacitance (*C*_{dl}) of the catalytic surface (Fig. S5, ESI[†]). It is worth noting that the *C*_{dl} of the product synthesized at 150 °C for 6 h is the highest but its OER performance is not the best, which may suffer from its poor crystallinity. The outstanding OER performance of the integrated CCHS/CP electrode is probably a result of the appropriate structure of the CCHS for OER and the synergistic effect between the CCHS and the CP.

Concerning the influence of morphology on the OER performance, there are some main points. Firstly, the size of the CCHS is in the micrometer scale, but it is assembled from nanoneedles which are on the nanometer scale. The assembled structure enables effective electrolyte transport, electron transfer, ion transport and active site accessibility. And the CCHS has good compatibility with electrolytes. The products synthesized at 150 °C for 15 h and 120 °C for 12 h agglomerate too tightly and they are too thick for effective electrolytic contact and active site accessibility while the products synthesized at 150 °C for 6 h and 180 °C for 12 h are too loose for effective electron transfer and ion transport. These results further demonstrate that the development of a nanostructure suitable for the highly efficient catalysis of OER is of paramount importance.

In summary, the CCHS assembled from nanoneedles could be synthesized using a facile one-step hydrothermal method. Time-dependent experiments were carried out to investigate the formation mechanism of the superstructure and a series of temperature and species control experiments (displayed in the ESI[†]) were also carried out. The linear scan voltammograms, Tafel slopes, EIS, and *C*_{dl} were tested to compare the electrochemically catalytic activities of products synthesized at different temperatures for different reaction times. The CCHS was found to be a good OER catalyst, achieving 10 mA cm⁻² at a low overpotential of merely ~240 mV. This is owing to the ordered 3D assembled superstructure with rough surface, increased electrochemically active surface area, accessibility of active sites and enhanced release of oxygen. In addition, the fabrication of the integrated CCHS/CP electrode could not only enhance the electron transport and exposed surface area, but also achieve a greater current density favorable for practical applications. Furthermore, this kind of CCHS could be used as catalysts in the growth of bamboo-like carbon nanotubes (displayed in the ESI[†]). Such a CCHS would be promising for applications in electrochemical devices and catalysis.

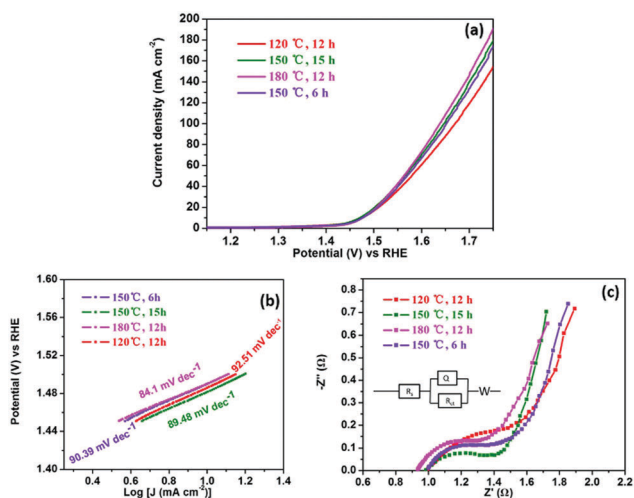


Fig. 4 (a) The polarization curves, (b) Tafel slopes, (c) EIS spectra of products synthesized at different temperatures or for different reaction times loaded on the CP.

This work was supported by NSFC (21431003, 21521091), China Ministry of Science and Technology under Contract of 2016YFA0202801.

Notes and references

- 1 F. Song and X. L. Hu, *J. Am. Chem. Soc.*, 2014, **136**, 16481–16484.
- 2 Y. Zhang, B. Cui, O. Derr, Z. Yao, Z. Qin, X. Deng, J. Li and H. Lin, *Nanoscale*, 2014, **6**, 3376–3383.
- 3 Y. X. Zhang, Q. Q. Xiao, X. Guo, X. X. Zhang, Y. F. Xue, L. Jing, X. Zhai, Y. M. Yan and K. N. Sun, *J. Power Sources*, 2015, **278**, 464–472.
- 4 Y. Lee, J. Suntivich, K. J. May, E. E. Perry and Y. Shao-Horn, *J. Phys. Chem. Lett.*, 2012, **3**, 399–404.
- 5 A. Bergmann, E. Martinez-Moreno, D. Teschner, P. Chernev, M. Glied, J. F. de Araújo, T. Reier, H. Dau and P. Strasser, *Nat. Commun.*, 2015, **6**, 8625–8634.
- 6 J. Zhao, Y. Zou, X. Zou, T. Bai, Y. Liu, R. Gao, D. Wang and G.-D. Li, *Nanoscale*, 2014, **6**, 7255–7262.
- 7 Y. Liang, Y. Li, H. Wang, J. Zhou, J. Wang, T. Regier and H. Dai, *Nat. Mater.*, 2011, **10**, 780–786.
- 8 S. Mao, Z. Wen, T. Huang, Y. Hou and J. Chen, *Energy Environ. Sci.*, 2014, **7**, 609–616.
- 9 T. Y. Ma, S. Dai, M. Jaroniec and S. Z. Qiao, *J. Am. Chem. Soc.*, 2014, **136**, 13925–13931.
- 10 M. W. Kanan and D. G. Nocera, *Science*, 2008, **321**, 1072–1075.
- 11 A. J. Esswein, M. J. McMurdo, P. N. Ross, A. T. Bell and T. D. Tilley, *J. Phys. Chem. C*, 2009, **113**, 15068–15072.
- 12 X. Lu and C. Zhao, *J. Mater. Chem. A*, 2013, **1**, 12053–12059.
- 13 J. Wu, Y. Xue, X. Yan, W. Yan, Q. Cheng and Y. Xie, *Nano Res.*, 2012, **5**, 521–530.
- 14 M. Tahir, N. Mahmood, X. Zhang, T. Mahmood, F. K. Butt, I. Aslam, M. Tanveer, F. Idrees, S. Khalid and I. Shakir, *Nano Res.*, 2015, **8**, 3725–3736.
- 15 J. Wu, Z. Ren, S. Du, L. Kong, B. Liu, W. Xi, J. Zhu and H. Fu, *Nano Res.*, 2016, **9**, 713–725.
- 16 Y. Wang, W. Ding, S. Chen, Y. Nie, K. Xiong and Z. Wei, *Chem. Commun.*, 2014, **50**, 15529–15532.
- 17 J. D. Costa, J. L. Lado, E. Carbó-Argibay, E. Paz, J. Gallo, M. F. t. Cerqueira, C. Rodríguez-Abreu, K. Kovnir and Y. V. Kolen'ko, *J. Phys. Chem. C*, 2016, **120**, 16537–16544.
- 18 X. Wang, Y. V. Kolen'ko, X. Q. Bao, K. Kovnir and L. Liu, *Angew. Chem., Int. Ed.*, 2015, **54**, 8188–8192.
- 19 J. L. Lado, X. Wang, E. Paz, E. Carbó-Argibay, N. Guldris, C. Rodríguez-Abreu, L. Liu, K. Kovnir and Y. V. Kolen'ko, *ACS Catal.*, 2015, **5**, 6503–6508.
- 20 X. Wang, Y. V. Kolen'ko and L. Liu, *Chem. Commun.*, 2015, **51**, 6738–6741.
- 21 L. Wang, C. Lin, D. Huang, F. Zhang, M. Wang and J. Jin, *ACS Appl. Mater. Interfaces*, 2014, **6**, 10172–10180.
- 22 K. Xu, P. Chen, X. Li, Y. Tong, H. Ding, X. Wu, W. Chu, Z. Peng, C. Wu and Y. Xie, *J. Am. Chem. Soc.*, 2015, **137**, 4119–4125.
- 23 J. Wang, H. X. Zhong, Z. L. Wang, F. L. Meng and X.-B. Zhang, *ACS Nano*, 2016, **10**, 2342–2348.
- 24 J. Yang, C. Yu, X. Fan, C. Zhao and J. Qiu, *Adv. Funct. Mater.*, 2015, **25**, 2109–2116.
- 25 J. Yang, C. Yu, X. Fan and J. Qiu, *Adv. Energy Mater.*, 2014, **4**, 1400761.
- 26 M. A. Garakani, S. Abouali, B. Zhang, C. A. Takagi, Z.-L. Xu, J.-q. Huang, J. Huang and J.-K. Kim, *ACS Appl. Mater. Interfaces*, 2014, **6**, 18971–18980.
- 27 N. Mahmood, M. Tahir, A. Mahmood, J. Zhu, C. Cao and Y. Hou, *Nano Energy*, 2015, **11**, 267–276.
- 28 S. Chen, J. Duan, M. Jaroniec and S. Z. Qiao, *Angew. Chem., Int. Ed.*, 2013, **52**, 13567–13570.
- 29 Z. Chen, H. Zhao, J. Zhang and J. Xu, *Sci. China Mater.*, 2016, **60**, 119–130.